Journal of Materials Chemistry A

Fluorescent polymer film with self-assembled three-dimensionally ordered nanopores: preparation, characterization and its application for explosives detection

Journal:	*Journal of Materials Chemistry A*
Manuscript ID:	TA-ART-05-2014-002554.R1
Article Type:	Paper
Date Submitted by the Author:	27-Jun-2014
Complete List of Authors:	Sun, Xiangcheng; University of Connecticut, Chemical and Biomolecular Engineering Department Bruckner, Christian; University of Connecticut, Department of Chemistry Nieh, Mu-Ping; University of Connecticut, Institute of Materials Science; University of Connecticut, Department of Chemical & Biomolecular Engineering Lei, Yu; University of Connecticut, Chemical and Biomolecular Engineering Department

Journal of

Materials Chemistry A

RSCPublishing

ARTICLE

Fluorescent polymer film with self-assembled three-dimensionally ordered nanopores: preparation, characterization and its application for explosives detection

Cite this: DOI: 10.1039/x0xx00000x

Received 00th January 2012,
Accepted 00th January 2012

DOI: 10.1039/x0xx00000x

www.rsc.org/

Xiangcheng Sun,[a] Christian Brückner,[b] Mu-Ping Nieh,[a,c] and Yu Lei[a*]

The sensitive and rapid detection of nitroaromatic explosives typically requires sophisticated sensor materials. We demonstrate here how a simple dip-coating process of a mixture of polystyrene and the fluorophore pyrene onto a glass slide generates a self-assembled fluorescent nanostructured film expressing regular breath-figure nanopores. Morphology investigations reveal that the fluorescent polymer films consist of a high-surface, three-dimensional nanoporous array of holes, enabling that the fluorescence of this material is rapidly and selectively quenched by nitroaromatic vapors. The morphology of the polymer was controlled by variation of the dip-coating parameters and the ratio of polystyrene to pyrene. This ratio also controls the fluorescence quenching efficiency of the material. We demonstrate the possible molecular origins of this through structural XRD studies as well as investigations of the electronic structure (optical properties, band gap and conduction band determinations) of the polymer film. Our results identify a novel high performance form of an otherwise known explosives sensing material. Most importantly, the findings point toward a general method for the facile realization of well-defined three-dimensional high surface sensor materials with optimized electronic properties.

Introduction

The reliable detection of explosives in the vapor phase is one of the pressing concerns in anti-terrorism efforts and in environmental pollution control measures.[1-8] The major contributors to the chemical fingerprinting of 2,4,6-trinitrotoluene (TNT)-based explosives are the more volatile byproducts 2,4-dinitrotoluene (DNT), 1,3-dinitrobenzene (DNB), and 4-nitrotoluene (4-NT).[9-11] Numerous analytical tools for explosive (nitroaromatics) detection have been developed, including trained canines[12, 13], mass spectrometry[14], ionization mass-spectroscopy[15], electrochemical sensors[16], optical sensors[17], and biosensors[3]. Among these detection methods, fluorescent sensing represents one of the most promising approaches for trace explosives detection due to the combination of a number of advantages: possible short response time, excellent sensitivity, and instrumental simplicity.[1, 18, 19] Sophisticated functional materials such as conjugated fluorescent polymers (CPs)[20, 21], quantum dots[22], microporous metal-organic frameworks (MOFs)[23, 24], and assembled monolayers of fluorophores[25, 26] were developed as high-performance fluorescence sensing materials. However, their applications are frequently hampered by the great synthetic efforts required to access them.

The quenching efficiency of most fluorescent sensory materials is heavily dependent on the film thickness that controls the diffusion of analyte vapors into the fluorescent film. For instance, Swager and coworkers[27] observed that for a fluorescent conjugated pentiptycene polymer the best fluorescence quenching was obtained with a film thickness of only 2.5 nm; the quenching efficiency was sharply decreased with the increase of the sensory film thickness. Such thin films are not always readily realized, however. Moreover, a sufficiently thick fluorescent film is required to produce a reliable signal intensity and to minimize the interference of photobleaching effects.[18]

To consolidate these seemingly diametrically opposed requirements, sensory materials with high surface-to-volume

ratios have been introduced.[28] For instance, we reported the use of polystyrene-pyrene-TBAH-based electrospun nanofibers that are capable of detecting a range of nitro-aromatics with ultrasensitivity. Their excellent sensing performance was attributed to an efficient long-range energy migration in the nanofibers but also to the large surface area to volume ratio of the nanofibrous membrane with high porosity. However, the fluorescence quenching mechanism in pyrene-polystyrene material by nitroaromatics was not fully understood.[29]

We report here a novel low-cost pyrene-polystyrene-based explosives sensing material, prepared by a single dip-coating step and that self-assembles into a film richly decorated with regular breath-figure nanoporous holes. This fluorescent high-surface film proved to be an excellent nitroaromatic vapor sensor. The unique high porosity morphology of the films was, however, only one factor for its high performance. Important was also the fine-tuning of the electronic structure of the material by the optimization of the degree of doping of the pyrene into the polymer matrix. Thus, our work illustrates two simple and generalizable mechanisms suited to substantially increase the sensing performance of polymeric sensor films.

Experimental

Materials

Polystyrene (PS, Mw = 350,000), tetrahydrofuran (THF, ≥ 99.0%), tetrabutylammonium hexafluorophosphate (TBAH, 98%) and acetonitrile (anhydrous, 99.8%) were purchased from Sigma-Aldrich. Pyrene (Py, 98%) was bought from Acros Organics. 2,4-dinitrotoluene (DNT, 97%), 1,3-dinitrobenzene (DNB), 4-nitrotoluene (4-NT), 3,5-dinitroaniline (DNA), urea, ammonium nitrate (AN), sodium nitrite (SN), chloranil (CA) were purchased from Sigma-Aldrich or Acros Organics. Perfume (Adidas, pure lightness; the main ingredients include alkanes, alcohols, parfum/fragrance and BHT) was bought from a local market. All the chemicals were used as received.

Preparation of Py-PS films

Py-doped PS films on glass slides were prepared by dip-coating. Briefly, polymer solutions with different Py concentrations (0.05 M, 0.1 M, and 0.2 M) and PS concentrations (from 0.5-wt % to 6-wt %) were first prepared with THF as the solvent. Next, glass slides (1.25 cm × 2.5 cm) were dipped into the fluorescence polymer solutions for 1 min, and then dried at room temperature in the chemical fume hood to generate fluorescent Py-PS sensing film consisting of 3D ordered nanoporous array of holes.

Fluorescence quenching experiments

The fluorescence quenching experiments were conducted in a similar method reported elsewhere.[28, 30] In brief, saturated DNT explosive vapors were generated in a sealed methacrylate cuvette containing a small amount of DNT powder, which was covered by a small piece of cotton wool. The glass slide with Py-PS film was then quickly inserted in the cuvette at a 45° angle, such that it was exposed to DNT vapor without making direct contact with the DNT powder. The fluorescence changes of Py-PS films were recorded continuously after the Py-PS films were inserted into the cuvette at time intervals of 30 s. Fluorescence emission spectra were measured in the range of 360-600 nm using a Varian Cary Eclipse fluorescence spectrometer (Agilent Technologies); $\lambda_{excitation}$ = 340 nm. The quenching efficiency was defined as $(I_0\text{-}I)/I_0$, where (I_0) is the first recorded fluorescent intensity of pyrene excimer peak right after the insertion of Py-PS film into cuvette and (I) is the corresponding fluorescent intensity at different exposure time. The quenching experiments upon the exposure of Py-PS film towards equilibrium vapors of other nitroaromatic compounds (DNB, NT, DNA) and common interferents (Urea, AN, SN, CA, perfume) were also performed in a similar way.

Characterization of Py-PS films

The morphology of as-prepared fluorescence Py-PS films were obtained using JEOL 6335F Field Emission scanning electron microscope (SEM) at an acceleration voltage of 10 kV, while surface topology images of the sensing films were examined by atomic force microscope (AFM, Asylum Research MFP-3d) in tapping mode with tip radius of 9 nm. Fluorescence microscopy images of Py-PS films were taken on a Nikon A1R confocal laser scanning microscope with attached photomultiplier tube (PMT) camera with an excitation of 405 nm. The thickness of the Py-PS films was measured by a Veeco Dektek 150 surface profiler. The X-ray diffraction (XRD) patterns were obtained on a Bruker D2 Phaser X-ray diffractometer using Cu Kα radiation at a rate of $0.01°\ 2\theta\ s^{-1}$ and operated at 15 kV and 10 mA. The absorption spectra of Py-PS films were performed on a Cary 50 UV-vis spectrophotometer (Agilent Technologies). As the UV-vis spectra of original Py-PS films were out of the detection range of spectrophotometer, all the absorption results were obtained from dip-coated films prepared in a similar way as described above except that 10-fold THF-diluted polymer solutions were used. Fluorescence emission spectra were measured using a Varian Cary Eclipse fluorescence spectrometer (Agilent Technologies). Electrochemical cyclic voltammetry (CV) were carried out with a CHI 601C electrochemical analyzer at a potential scan rate of 50 mV/s in acetonitrile consisting of 0.1 mol/L TBAH. Py-PS thin film dip-coated on the glassy carbon electrode were used as the working electrode, while Pt wire and Ag/AgCl electrode served as the counter and reference electrodes, respectively. Prior to each CV measurement, the solutions were deoxygenated with nitrogen.

Results and discussion

Preparation and Morphology of Py-PS fluorescent film

In a typical preparation of our pyrene-polystyrene (Py-PS) films, a solution of 0.1 M Py and 4-wt% PS of average Mw 350,000 in THF was dip-coated on a standard microscopy glass slide. During the drying step of the dip-coating process, the relative humidity was controlled to ~60% at an airflow velocity

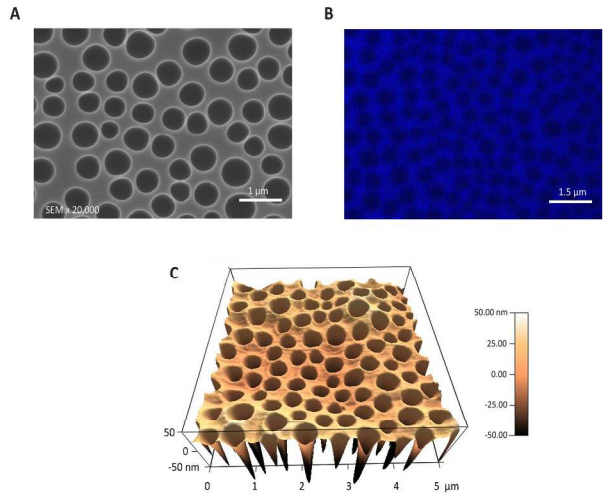

Figure 1. Morphology of Py-PS fluorescent film with three-dimensionally ordered nanoporous array. (A) SEM image of nanoporous Py-PS film with an average pore size of 400 nm. (B) Confocal fluorescence microscope image of nanoporous fluorescent film. (C) 3D-AFM image of nanoporous array film collected in tapping mode for 5 × 5 µm section.

of about 35 m/min. Figure 1 shows the morphology of a typical polymer film thus prepared. Closely spaced 3D nanoporous array of holes are observed (Figure 1A), with the spacing between pores in the range of hundreds nanometers, providing a high porosity and surface area to the as-prepared film. A confocal fluorescence microscopy image of the film (Figure 1B) indicates that the film is fluorescent, with the holes appearing to be darker and less fluorescing. Figure 1C shows a 3D-AFM image of the film, revealing a pore size of ~ 400 nm.

This formation of 3D ordered array of nanopores in membranes was achieved applying the "breath figures" principles.[31-34] Breath figures are proposed to form through the condensation of water vapor on the surface of a polymer/organic solvent solution. As the water droplets are uniformly packed in the film by capillary force, it leads to the formation of 3D ordered array of nanoholes in polymer film after the solvent and water evaporates. Generally, the solvents used in preparing this kind of nanoporous film are highly volatile and water-immiscible.[35, 36] However, the groups of Kim and Raczkowska[37, 38] have recently shown that breath figures can also be obtained using water-miscible solvents such as THF used here. The selection of the appropriate molecular weight of linear polystyrenes is also an important factor in the formation of regular holes in polymer film, as recently observed by Han et al..[39] Interestingly, when pyrene was added to the polystyrene solution, it might work as an additive that promoted the formation of ordered breath fingers as observed in other reports.[36] A film prepared from a solution of 4-wt% PS and 0.1 M Py shows the well-ordered expression of the breath figures, while in the absence or reduction of the pyrene, the orderliness of nanoporous array in polymer film is poor. The SEM images and calculated pore density of a series of nanoporous fluorescent films are presented in Supporting Information (see Figure S1 and Table S1). Furthermore, pore size and dimensions of the nanopores were also greatly dependent on the humidity and velocity of airflow across the surface.[32] It was previously reported that the size and number of pores, spacing between pores and film thickness can be tuned by factors such as polymer concentration, additive, solvent, temperature, humidity, preparation methods, etc.[32, 35, 40] Therefore, it is expected that through careful control of composition and evaporation conditions, especially the doping of the polymer with various fluorophores, a broad range of 3D ordered nanoporous fluorescent films can be prepared for a variety of sensing applications.

For solid-state sensing films, thickness plays a pivotal role, mainly due to the diffusion resistance of analyte vapors into the film.[27] The thickness of the dip-coated fluorescent polymer film in our study was about 2 µm, as measured by Dektek surface profiler. The overall film thickness is much higher than those of other reported fluorescent sensing films[6], but owing to its nanoporous surface structure, it possesses a comparable, if not better, sensing performance than much thinner films.

Sensing performance of the pyrene-doped polystyrene film

Figure 2A shows the time-dependent fluorescence spectra of a Py-PS film, prepared as described above. The emission peak at ~470 nm is assigned to originate from the pyrene excimer. Upon exposure of the film to saturated DNT vapor at ambient temperature, the fluorescence of the excimer is quenched by 35% within 2 min, by ~60% within 6 min, and after 30 min by about 90%. As a comparison, a smooth film of the same composition but prepared using evaporation conditions that did not allow the formation of the breath-figures, shows a slower response and overall ~20% lower quenching efficiency upon exposure to saturated DNT vapor.

The fluorescence quenching mechanism relies primarily on the photo-induced electron transfer (PET) from the excited pyrene excimers within the Py-PS films to the electron-deficient nitroaromatics.[6, 28] This is also supported by the relative positions of the computed frontier orbitals of the molecules involved (see below, Table S2 and discussion in Supporting Information). The lack of spectral overlap between the DNT absorbance and Py-PS film emission excludes the probability of energy transfer from the excited film to DNT.[18] The presence of excimer emissions from Py-PS film shows that the loading of pyrene is high enough to form π-stacked Py dimers. The shape-persistent geometry of the PS scaffold presumably enables effective co-facial π-π stacking, allowing pyrene monomer and/or excimer units possible to be inserted in and between the phenyl groups of PS, thus contributing to the formation of extended conjugation of π electrons and efficient long-range energy migration in the Py-PS films.[6, 28]

Selectivity is one crucial criterion in sensing (Figure 2C). Remarkable quenching efficiency was observed for the sensing

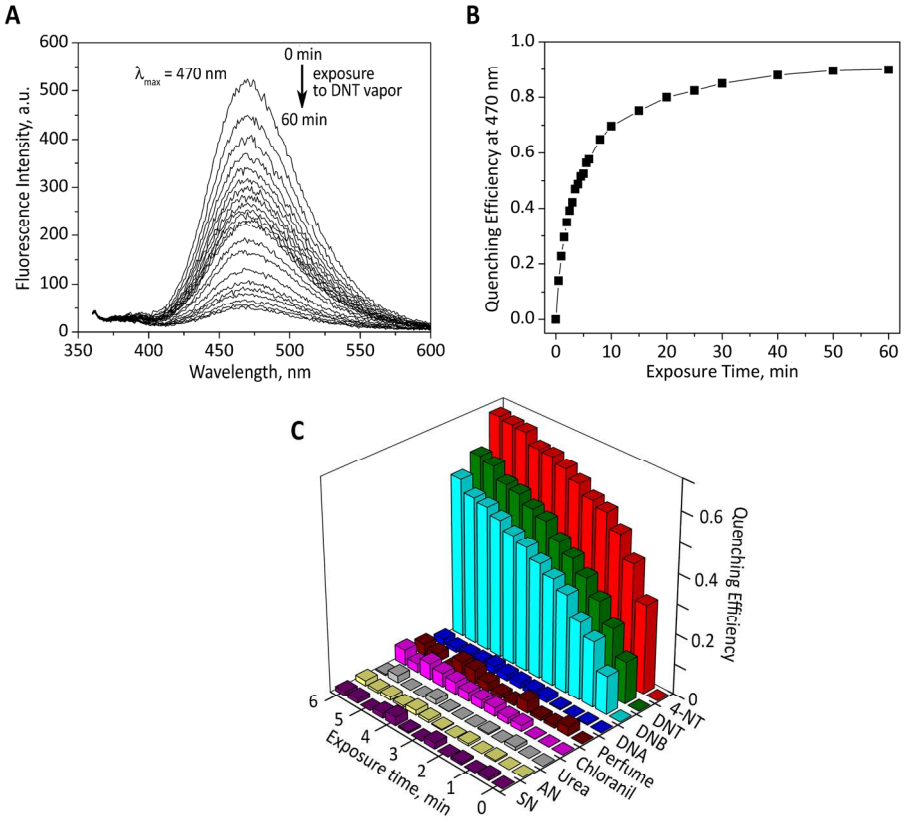

Figure 2. Fluorescence quenching profiles of 3D nanoporous Py-PS fluorescent film (0.1 M Py and 4-wt % PS). (A) The time-dependent fluorescence intensity upon exposure to equilibrium DNT vapor (the exposure time from top to bottom is 0, 0.5, 1, 1.5, 2, 2.5, 3, 3.5, 4, 4.5, 5, 5.5, 6, 8, 10, 15, 20, 25, 30, 40, 50, 60 min, respectively). (B) The time-dependent fluorescence quenching efficiency of 3D nanoporous Py-PS film at 470 nm exposed to saturated DNT vapor; (C) The time-dependent fluorescence quenching efficiency at Py excimer peak upon exposure of 3D nanoporous Py-PS film to saturated vapors of different analytes.

film when exposed to nitroaromatic vapors such as 4-NT (68%), DNT (60%) and DNB (53%; values reported for the quenching of the pyrene excimer band after 6 min exposure to air saturated with nitroaromatic vapors at ambient temperature). The differences in the relative quenching efficiencies can be rationalized based on a combination of the electron acceptance ability and vapor pressure of the nitroaromatics tested (see Supporting Information Table S2 and discussion there). Exposure to more electron-rich aromatic compounds such as 3,5-dinitroaniline (DNA) and commercial perfume did not lead to a significant fluorescence quenching. The absence of any significant quenching of the nanoporous Py-PS film upon exposure to strong electron-acceptors such as chloranil indicated that the fluorescent films were inert to this strong oxidant. Commonly used nitrogen fertilizers such as urea, ammonium nitrate (AN) and sodium nitrite (SN) induce only negligible quenching. The results show that Py-PS films exhibit selectivity towards the identification of nitroaromatic explosive compounds.

The Role of Pyrene Doping on the Sensing Ability of the Py-PS Film

To investigate the role of Py-doping on the quenching efficiency of the sensing film upon exposure to DNT, we performed studies on films prepared of solutions of varying polystyrene and pyrene concentrations. Figure 3 presents the results, demonstrating that both the PS and Py concentrations in the solutions (the films were prepared from by dip-coating) have a significant impact on quenching efficiency. In one series (Figure 3A), the pyrene concentration was fixed at 0.1 M and films from PS solutions of varying concentrations (from 0-wt% to 6-wt%) were prepared. As the PS concentration increases (from 0-wt% to 4-wt%), the quenching efficiency (after 6 min) increases to a maximum of 60%. Further increase of PS concentration to 6% reduces the quenching efficiency to 42%. Consequently, 4-wt% of PS was selected for subsequent study of the effect of Py concentration.

At a fixed PS concentration of 4-wt%, the quenching efficiencies for Py-PS films prepared with pyrene concentration varying from 0.05 to 0.2 M, were 33%, 60%, and 36% after a 6 min exposure to saturated DNT vapor (Figure 3B), indicating that the combination of 4-wt% PS and 0.1 M pyrene generated the best DNT sensing film. The possible molecular origin of the performance differences will be discussed below.

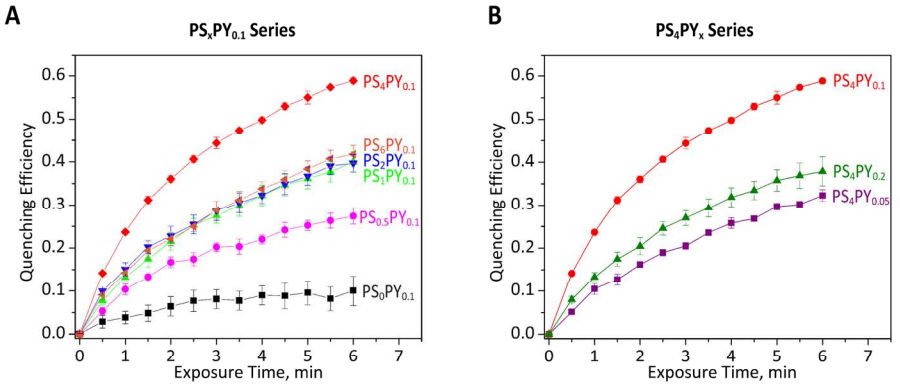

Figure 3. Effect of composition of dipping coating solution on fluorescent quenching efficiencies. (A) The effect of PS concentration (with 0.1 M Py fixed) on time-dependent fluorescence quenching efficiency upon exposure of film to saturated DNT vapor at Py excimer peak; (B) The effect of Py concentration (with 4-wt% PS fixed) on time-dependent fluorescence quenching efficiency upon exposure of film to saturated DNT vapor at Py excimer peak. Different Py-PS fluorescent films were prepared using different Py and PS concentrations. The subscript of PS in PS_xPY_z indicates the wt% of PS while the subscript of PY in PS_xPY_z indicates the molar concentration of pyrene (e.g., the $PS_4PY_{0.1}$ film was prepared using 4-wt% PS and 0.1 M pyrene in THF).

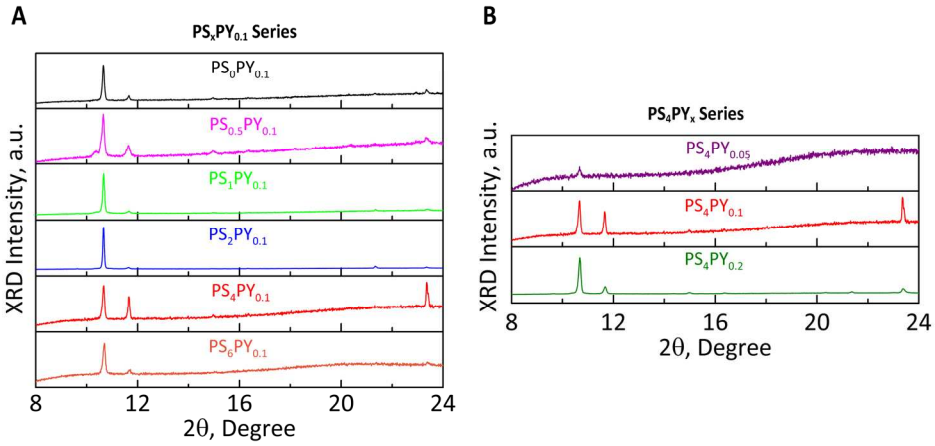

Figure 4. *θ-2θ* X-ray diffraction (XRD) spectra of a series of (A) $PS_xPY_{0.1}$ and (B) PS_4PY_z fluorescent films. The signals at ~10.70°, ~11.65° and ~23.35° can be assigned to the (001), (110) and (220) peaks of pyrene crystals.

XRD Patterns of Py-PS fluorescent films

XRD patterns provide a direct signature of regular order, and any observed layer d-spacing can be compared to the molecular dimensions for the determination of likely molecular arrangements.[41] Thus, the degree of crystallinity of pyrene in polystyrene can be studied by analysis of the XRD patterns. Any spatial restriction of pyrene is known to influence excimer formation.[42] The XRD patterns obtained for the films (Figure 4) indicate the existence of pyrene crystallites in the Py-PS composites films (the peaks observed can be assigned to the (001), (110) and (220) peaks of pyrene; ICDD No. 00-024-1855), while amorphous polystyrene served as a hydrophobic matrix for pyrene crystal growth. The d spacing derived here from the 110 and 220 peaks is 7.59 and 3.80 Å, respectively. The d-spacing of 3.80 Å is in good agreement with the reported face-to-face pyrene stack distance value of ~ 3.18- 3.49 Å.[42, 43] The ratios of peak intensity assigned to pyrene crystallites do not increase monotonically with the variation of the PS to Py ratio used to form the films (see Table 1 for a listing of the I(110)/I(001) and I(220)/I(001) ratios).

However, it is likely of relevance to note that the system of best sensing performance, the $PS_4PY_{0.1}$ film, is also the film with the apparent highest degree of pyrene crystallinity. Evidently, the approximate 1:4 molar pyrene ring: styrene ratio of this film is conducive of forming pyrene crystallites and presumably also supports the organization of the pyrene into functional excimers. Wang et al.[28] reported that the shape-persistent geometry of the PS scaffold could potentially enable effective co-facial π-π stacking, allowing pyrene monomer and excimer units possible to be inserted in and between the phenyl groups of the PS chains. Swager and co-workers proposed and demonstrated that one-dimensional π-π stacking is highly

favorable for exciton transportation via co-facial intermolecular electronic coupling ("molecular wire" amplification).[44] In this study, one-dimensional pyrene and excimers doped into polystyrene similar to that of pyrene salt might be formed[43, 45], and thus results in a facilitated long-range exciton migration and achieves amplified fluorescence quenching similar to "molecular wire".

Table 1. Summary of structural, optical, electrochemical, and frontier orbital properties of Py-PS fluorescent films of varying composition

Py-PS Films	$I_{(110)}/I_{(001)}$	$I_{(220)}/I_{(001)}$	I_{ex}/I_{mon} [a]	E_g^{opt}(eV) [b]	E_{ox}'(V) [c]	E_{HOMO} (eV)	E_{LUMO} (eV) [d]
$PS_0PY_{0.1}$	0.12	0.11	2.75				
$PS_{0.5}PY_{0.1}$	0.26	0.13	4.33	3.27	0.99	-5.39	-2.12
$PS_1PY_{0.1}$	0.05	0.02	6.02	3.49	1.04	-5.44	-1.95
$PS_2PY_{0.1}$	0.03	0.02	8.77	3.52	1.07	-5.47	-1.95
$PS_4PY_{0.1}$	0.68	0.74	14.32	3.56	1.08	-5.48	-1.92
$PS_6PY_{0.1}$	0.15	0.09	6.60	3.57	1.22	-5.62	-2.05
$PS_4PY_{0.05}$	-	-	3.69	3.57	1.30	-5.70	-2.13
$PS_4PY_{0.2}$	0.19	0.12	7.06	3.54	1.19	-5.59	-2.05

[a] I_{ex} was obtained using excimer peak intensity at ~470 nm while I_{mon} was the peak intensity at ~395 nm. [b] Optical band gap is estimated from the low-energy band edge of the UV-vis spectrum (see Fig. 6). The absorption results were obtained using dip-coating films of original solutions diluted by a factor of 10 because the UV-vis spectra of original Py-PS films are out of the detection range of the spectrophotometer used. The experiments were conducted at least three times and the fits were performed three times, and average value was reported, error was less than 0.005 eV, linear fitting R square was larger than 0.98. [c] Estimated onset potential of oxidation from the cyclic voltammetry results. [d] LUMO values calculated from the band gap and HOMO values.

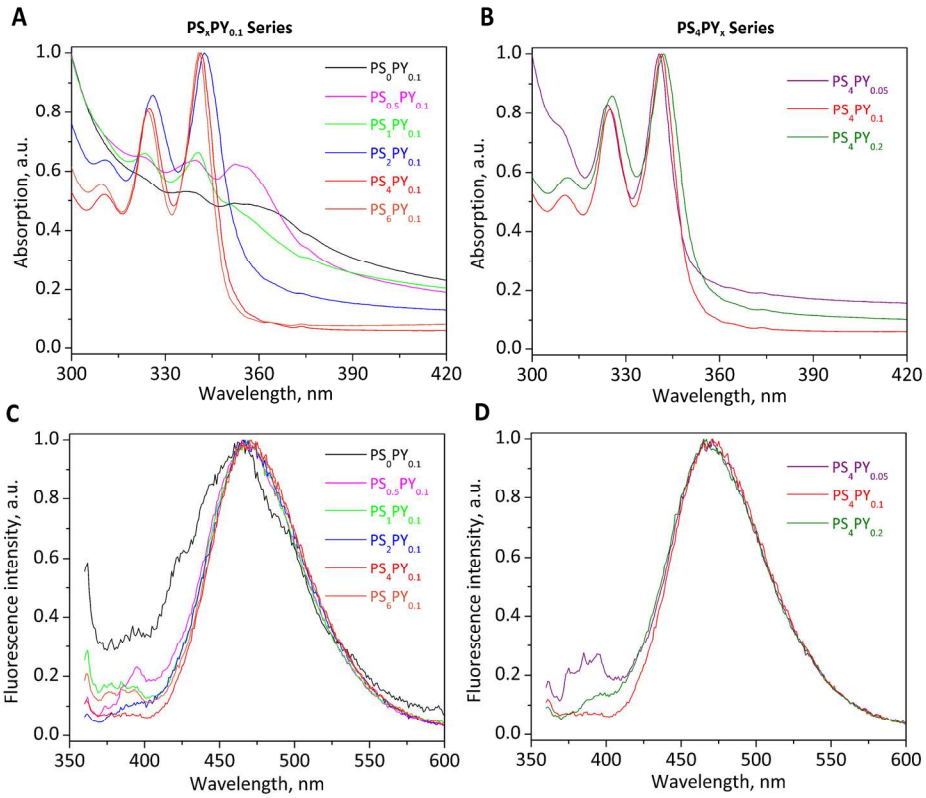

Figure 5. Absorption and emission spectra of a series of $PS_xPY_{0.1}$ and PS_4PY_z fluorescent films. (A) and (B) Normalized absorption spectra of a series of $PS_xPY_{0.1}$ and PS_4PY_z fluorescent films, respectively (prepared with 10× dilution solution because the UV-vis spectra of original Py-PS films are out of the detection range of spectrophotometer). (C) and (D) Normalized emission spectra of a series of $PS_xPY_{0.1}$ and PS_4PY_z fluorescent films, respectively.

Optical properties of Py-PS fluorescent films

The absorption and fluorescence spectra of thin films of different composition are shown in Figure 5, and the corresponding data are also summarized in Table 1. The absorption spectra of Py-PS films showed the characteristic three bands at about 311, 325 and 342 nm, corresponding to the vibrational bands of the $S_0 \rightarrow S_2$ transition of pyrene ring.[28] Furthermore, two small peaks can also be observed at 355 nm and 373 nm, which correspond to the vibronic bands of $S_0 \rightarrow S_1$ transition of pyrene rings.[46] At constant Py concentration (from $PS_0PY_{0.1}$ to $PS_6PY_{0.1}$), a shift of the absorption peaks was observed, indicating a changing degree of interaction between the pyrene units in the polymer.[42, 47]

The UV-vis spectra also allow the estimation of the optical absorption band gap.[48, 49] The optical band gap of the polymer can be calculated using Eq. 1, with A being the absorbance and E_g is the band gap corresponding to a particular absorption of photon energy hν.[50] The values of the direct optical band gap are determined by the extrapolation of the linear region to zero absorption (Ahν = 0).

$$Ah\nu = (h\nu - E_g)^{1/2} \qquad \text{Eq. 1}$$

The extrapolating graphs are shown in Fig. 6 and the data derived are summarized in Table 1. Thus, the optical band gap changed with PS and Py concentrations. These band gap changes are further confirmed by nonsymmetric increases in the highest occupied molecular orbital (HOMO) and lowest unoccupied molecular orbital (LUMO) energies discussed below, similar to the finding reported by Facchetti and co-workers.[51]

The dependence of the pyrene concentration in the polymer on the excimer formation[29] was determined by examining the fluorescence ratio of the pyrene excimer (I_{ex}, at 470 nm) to pyrene monomer emission (I_{mon}, at 395 nm) (I_{ex}/I_{mon}). The data are presented in Table 1. Higher I_{ex}/I_{mon} ratios suggest that the pyrenes are located more closely to one another[47], which benefits the fluorescence quenching of pyrene, increasing the sensitivity of explosives detection[29]. This ratio is 14.3 for the film made of 0.1 M Py and 4 wt % PS. A reduction or increase of the pyrene-styrene ratios leads to a degradation of the I_{ex}/I_{mon} ratios ranging from 2.75 to 8.77 (Table 1), again indicating that the efficiency of the excimer formation in $PS_4PY_{0.1}$ film is much higher than in other films. The result here corroborates the XRD data and confirms that $PS_4PY_{0.1}$ film possesses the highest degree π-π stacking of pyrene in PS.

Electrochemical characterization of Py-PS fluorescent films

Cyclic Voltammetry is a dynamic electrochemical method to determine the redox behaviour as well as to estimate the HOMO and LUMO energy levels of the materials under investigation.[52] The oxidation process corresponds to the removal of electron from the HOMO energy level, while the reduction potential corresponds to the LUMO energy level of the materials. To provide a better insight about the relative energies of the orbitals of Py-PS composite polymers, and thus the feasibility of the energy transfer, we carried out cyclic voltammetry studies with dip-coated film on glassy carbon electrodes to obtain the oxidation potentials (E_{ox}') (Figure 7). According to the empirical relationship proposed by Bredas et al. based on a detailed comparison between valence effective Hamiltonian calculations and experimental electrochemical measurements[53], the solid state HOMO level correlates to E_{ox}' (vs. SCE), the onset potentials of oxidation process of the polymer (Eq. 2). The onset potentials are determined from the intersection of the two tangents drawn at the rising current and baseline charging current of the CV traces.[54] The relation can be expressed as

$$HOMO = -(E_{ox}' + 4.4)eV \qquad \text{Eq. 2}$$

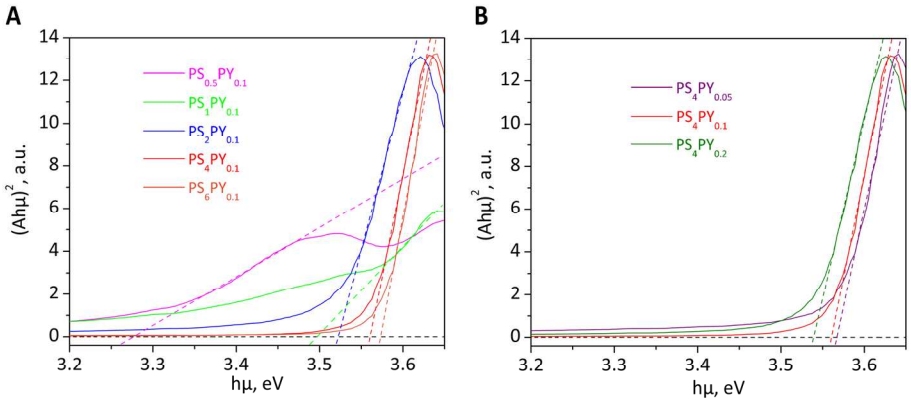

Figure 6. $(Ah\nu)^2$ versus the photon energy hν. The extrapolation of the linear region to zero absorption allows us to determine gap energy of Py-PS fluorescent films (the data from Figure 5 A, B).

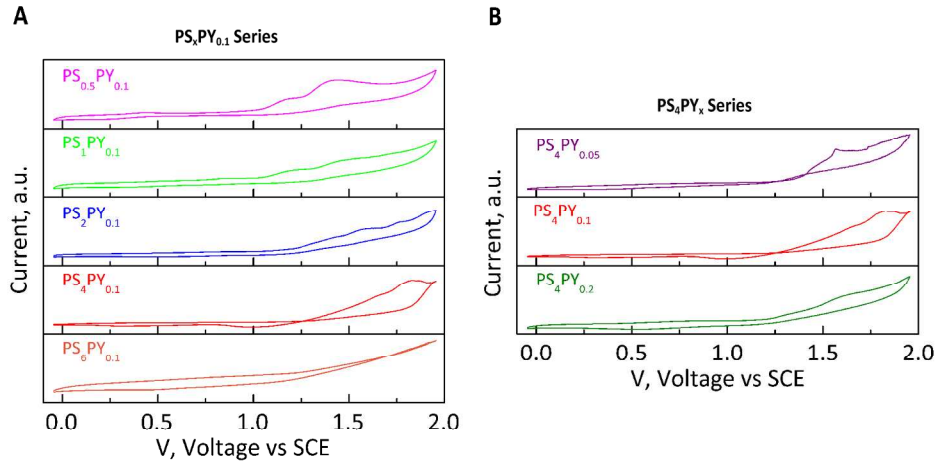

Figure 7. Cyclic voltammograms of a series of (A) $PS_xPY_{0.1}$ and (B) PS_4PY_z fluorescent films in acetonitrile with 0.1mol/L TBAH at a scan rate of 50 mV/s.

The onset oxidation potentials and valence band of Py-PS films were obtained using the CVs shown in Figure 7. We observed that the valence band can be tuned through doping Py into polymers. For the Py-PS films prepared with fixed Py concentration, the valence band decreases with the increase of PS concentrations, while the band gap increases (as determined optically, see above). Both the change of band gap and the change of valence band follow an asymmetric trend, and thus the conduction band of fluorescent films demonstrates a different trend. If the distinction between optical and electronic band gap is ignored, the conduction band can be obtained by adding the valence band and the optical band gap.[55-57] The conduction band of $PS_4PY_{0.1}$ film was highest, with a value of -1.92 eV, which explains its best quenching efficiency upon exposure to DNT. The LUMO of DNT is -3.22 eV. The driving force of PET process for DNT quenching on $PS_4PY_{0.1}$ film thus was ~ 1.30 eV. The conduction bands of the various fluorescent films studied were ranged from -1.92 eV to -2.13 eV. The LUMO level of the nitroaromatics studied in this research was lower than the estimated LUMO of fluorescent films, validating that a PET processes is the molecular origin of the fluorescence quenching (Figure S2, see Supporting Information).

Conclusions

In this study, a novel 3D nanoporous fluorescent film was prepared via simple dip-coating of PS and Py solutions, and then its application for the sensitive and selective detection of explosive vapor was investigated, whereby we optimized the sensing film with respect to morphology and electronic properties by varying the pyrene : styrene molar ratios. Upon exposure of the best sensing film ($PS_4PY_{0.1}$) to saturated DNT vapor, the fluorescence quenching of excimer peak at 470 nm was observed to be 60% within 6 min and to reach a plateau of 90% after 30 min. The sensing Py-PS films possess an excellent selectivity against common interferents.

This study is, to the best of our knowledge, the first report of a novel self-assembled 3D nanoporous array fluorescent film via a simple dip-coating preparation method that is utilized for sensitive and selective detection of nitro explosives. The presence of three-dimensional nanoporous array of holes in fluorescent film enables a high porosity and fast quenching efficiency upon exposure to explosive vapor. In addition, characterization of the as-prepared films using XRD, UV-vis and fluorescence spectroscope, and cyclic voltammetry indicated that the crystal structure of pyrene in Py-PS film, electronic structure, band gap and conduction band of fluorescent polymer film can be tuned via the pyrene-doping degree. This, in turn, results in the variation of the fluorescence quenching efficiency of the sensor. This study may provide insights into the design of novel nanostructured sensing polymer doped with small fluorophore molecules and the present findings offer a new research direction for the design of three-dimensionally organized nanoporous fluorescent sensing films.

Acknowledgements

This work was financially supported by the National Science Foundation and the University of Connecticut Prototype Fund. We thank Professors Douglas Adamson, George Rossetti, Jr., and Jing Zhao for the helpful discussions. We also acknowledge Drs. Lichun Zhang, Carol Norris, Vincent Palumbo and Mr. Jack Gromek for technical support.

Notes and references

[a] Department of Chemical and Biomolecular Engineering, University of Connecticut, Storrs, Connecticut 06269-3222, USA.
[b] Department of Chemistry, University of Connecticut, Storrs, Connecticut 06269-3060, USA.
[c] Institute of Materials Science, University of Connecticut, Storrs, Connecticut 06269-3136, USA.
* Address correspondence to: ylei@engr.uconn.edu
Electronic Supplementary Information (ESI) available: [details of any supplementary information available should be included here]. See DOI: 10.1039/b000000x/

1. A. Rose, Z. Zhu, C. F. Madigan, T. M. Swager and V. Bulovic, *Nature*, 2005, **434**, 876-879.
2. S. J. Toal and W. C. Trogler, *J. Mater. Chem.*, 2006, **16**, 2871-2883.
3. V. Radhika, T. Proikas-Cezanne, M. Jayaraman, D. Onesime, J. H. Ha and D. N. Dhanasekaran, *Nat. Chem. Biol.*, 2007, **3**, 325-330.
4. Y. Salinas, R. Martinez-Manez, M. D. Marcos, F. Sancenon, A. M. Costero, M. Parra and S. Gil, *Chem. Soc. Rev.*, 2012, **41**, 1261-1296.
5. H. H. Nguyen, X. Li, N. Wang, Z. Y. Wang, J. Ma, W. J. Bock and D. Ma, *Macromolecules*, 2009, **42**, 921-926.
6. G. B. Demirel, B. Daglar and M. Bayindir, *Chem. Commun.*, 2013, **49**, 6140-6142.
7. Y. Che, D. E. Gross, H. Huang, D. Yang, X. Yang, E. Discekici, Z. Xue, H. Zhao, J. S. Moore and L. Zang, *J. Am. Chem. Soc.*, 2012, **134**, 4978-4982.
8. P. Anzenbacher, L. Mosca, M. A. Palacios, G. V. Zyryanov and P. Koutnik, *Chem. Eur. J.*, 2012, **18**, 12712-12718.
9. C. J. Cumming, C. Aker, M. Fisher, M. Fox, M. J. la Grone, D. Reust, M. G. Rockley, T. M. Swager, E. Towers and V. Williams, *IEEE Trans. Geosci. Remote Sens.*, 2001, **39**, 1119-1128.
10. A. Lan, K. Li, H. Wu, D. H. Olson, T. J. Emge, W. Ki, M. Hong and J. Li, *Angew. Chem. Int. Ed.*, 2009, **48**, 2334-2338.
11. X. Sun, Y. Liu, S. Mopidevi, Y. Meng, F. Huang, J. Parisi, M.-P. Nieh, C. Cornelius, S. L. Suib and Y. Lei, *Sens. Actuators B*, 2014, **195**, 52-57.
12. K. G. Furton and L. J. Myers, *Talanta*, 2001, **54**, 487-500.
13. J. Yinon, *Anal. Chem.*, 2003, **75**, 98 A-105 A.
14. D. R. Ifa, N. E. Manicke, A. L. Dill and G. Cooks, *Science*, 2008, **321**, 805-805.
15. G. A. Eiceman, E. V. Krylov, E. G. Nazarov and R. A. Miller, *Anal. Chem.*, 2004, **76**, 4937-4944.
16. J. Wang, M. Pumera, M. P. Chatrathi, A. Escarpa, M. Musameh, G. Collins, A. Mulchandani, Y. H. Lin and K. Olsen, *Anal. Chem.*, 2002, **74**, 1187-1191.
17. M. E. Germain and M. J. Knapp, *Chem. Soc. Rev.*, 2009, **38**, 2543-2555.
18. T. Naddo, Y. Che, W. Zhang, K. Balakrishnan, X. Yang, M. Yen, J. Zhao, J. S. Moore and L. Zang, *J. Am. Chem. Soc.*, 2007, **129**, 6978-6979.
19. Y. Wang, A. La, C. Brueckner and Y. Lei, *Chem. Commun.*, 2012, **48**, 9903-9905.
20. S. W. Thomas, III, G. D. Joly and T. M. Swager, *Chem. Rev.*, 2007, **107**, 1339-1386.
21. S. Rochat and T. M. Swager, *ACS Appl. Mater. Interfaces*, 2013, **5**, 4488-4502.
22. R. Freeman, T. Finder, L. Bahshi, R. Gill and I. Willner, *Adv. Mater.*, 2012, **24**, 6416-6421.
23. S. Pramanik, C. Zheng, X. Zhang, T. J. Emge and J. Li, *J. Am. Chem. Soc.*, 2011, **133**, 4153-4155.
24. S. S. Nagarkar, B. Joarder, A. K. Chaudhari, S. Mukherjee and S. K. Ghosh, *Angew. Chem. Int. Ed.*, 2013, **52**, 2881-2885.
25. G. He, G. Zhang, F. Lue and Y. Fang, *Chem. Mater.*, 2009, **21**, 1494-1499.
26. L. Ding, Y. Liu, Y. Cao, L. Wang, Y. Xin and Y. Fang, *J. Mater. Chem.*, 2012, **22**, 11574-11582.
27. J. S. Yang and T. M. Swager, *J. Am. Chem. Soc.*, 1998, **120**, 5321-5322.
28. Y. Wang, A. La, Y. Ding, Y. Liu and Y. Lei, *Adv. Funct. Mater.*, 2012, **22**, 3547-3555.
29. H.-S. Jang, Y. Wang, Y. Lei and M.-P. Nieh, *J. Phys. Chem. C*, 2013, **117**, 1428-1435.
30. D. Zhao and T. M. Swager, *Macromolecules*, 2005, **38**, 9377-9384.
31. G. Widawski, M. Rawiso and B. Francois, *Nature*, 1994, **369**, 387-389.
32. M. Srinivasarao, D. Collings, A. Philips and S. Patel, *Science*, 2001, **292**, 79-83.
33. T. Hayakawa and S. Horiuchi, *Angew. Chem. Int. Ed.*, 2003, **42**, 2285-2289.
34. U. H. F. Bunz, *Adv. Mater.*, 2006, **18**, 973-989.
35. M. H. Stenzel, C. Barner-Kowollik and T. P. Davis, *J. Polym. Sci. A Polym. Chem.*, 2006, **44**, 2363-2375.
36. E. Ferrari, P. Fabbri and F. Pilati, *Langmuir*, 2011, **27**, 1874-1881.
37. M. S. Park and J. K. Kim, *Langmuir*, 2004, **20**, 5347-5352.
38. W. Madej, A. Budkowski, J. Raczkowska and J. Rysz, *Langmuir*, 2008, **24**, 3517-3524.
39. J. Peng, Y. Han, Y. Yang and B. Li, *Polymer*, 2004, **45**, 447-452.
40. B. You, L. Shi, N. Wen, X. Liu, L. Wu and J. Zi, *Macromolecules*, 2008, **41**, 6624-6626.
41. L. A. Lucas, D. M. DeLongchamp, L. J. Richter, R. J. Kline, D. A. Fischer, B. R. Kaafarani and G. E. Jabbour, *Chem. Mater.*, 2008, **20**, 5743-5749.
42. J. You, J. A. Yoon, J. Kim, C.-F. Huang, K. Matyjaszewski and E. Kim, *Chem. Mater.*, 2010, **22**, 4426-4434.
43. S. Lee, B. L. Chen, D. C. Fredrickson, F. J. DiSalvo, E. Lobkovsky and J. A. Adams, *Chem. Mater.*, 2003, **15**, 1420-1433.
44. T. M. Swager, *Acc. Chem. Res.*, 1998, **31**, 201-207.
45. T. Devic, M. Yuan, J. Adams, D. C. Fredrickson, S. Lee and D. Venkataraman, *J. Am. Chem. Soc.*, 2005, **127**, 14616-14627.
46. M. Vybornyi, A. V. Rudnev, S. M. Langenegger, T. Wandlowski, G. Calzaferri and R. Häner, *Angew. Chem. Int. Ed.*, 2013, **52**, 11488-11493.
47. V. D. Deepak and S. K. Asha, *J. Phys. Chem. B*, 2009, **113**, 11887-11897.
48. Y. Zhu, M. M. Alam and S. A. Jenekhe, *Macromolecules*, 2002, **35**, 9844-9846.
49. K. Kawasumi, Q. Zhang, Y. Segawa, L. T. Scott and K. Itami, *Nat. Chem.*, 2013, **5**, 739-744.
50. J. Tauc, R. Grigorovici and A. Vancu, *Phys. Status Solidi B*, 1966, **15**, 627-637.
51. H. Usta, C. Risko, Z. Wang, H. Huang, M. K. Deliomeroglu, A. Zhukhovitskiy, A. Facchetti and T. J. Marks, *J. Am. Chem. Soc.*, 2009, **131**, 5586-5608.
52. Y. F. Li, Y. Cao, J. Gao, D. L. Wang, G. Yu and A. J. Heeger, *Synth. Met.*, 1999, **99**, 243-248.
53. J. L. Bredas, R. Silbey, D. S. Boudreaux and R. R. Chance, *J. Am. Chem. Soc.*, 1983, **105**, 6555-6559.
54. Z. K. Chen, W. Huang, L. H. Wang, E. T. Kang, B. J. Chen, C. S. Lee and S. T. Lee, *Macromolecules*, 2000, **33**, 9015-9025.
55. S. W. Hwang and Y. Chen, *Macromolecules*, 2002, **35**, 5438-5443.
56. S. Hwang, J. H. Lee, C. Park, H. Lee, C. Kim, C. Park, M.-H. Lee, W. Lee, J. Park, K. Kim, N.-G. Park and C. Kim, *Chem. Commun.*, 2007, 4887-4889.
57. M. Suresh, A. K. Mandal, E. Suresh and A. Das, *Chem. Sci.*, 2013, **4**, 2380-2386.